From in vitro evaluation of a finite element model of the spine to in silico comparison of spine instrumentations

Claudio Vergari, Mathilde Gaume, Sylvain Persohn, Lotfi Miladi, Wafa Skalli

Accepted Manuscript. Published in Journal of the Mechanical Behavior of Biomedical Materials.
DOI : https://doi.org/10.1016/j.jmbbm.2021.104797

From In Vitro Evaluation of a Finite Element Model of the Spine to In Silico Comparison of Spine Instrumentations

Claudio Vergari *[a], Mathilde Gaume [b], Sylvain Persohn, [a], Lotfi Miladi [b], Wafa Skalli [a]

Abstract

Growth-preserving spinal surgery suffer from high complications rate. A recent bipolar instrumentation using two anchoring points (thoracic and pelvic) showed lower rates, but its biomechanical behaviour has not been characterised yet. The aim of this work was to combine in vitro and in vivo data to improve and validate a finite element model (FEM) of the spine, and to apply it to compare bipolar and classical all-screws implants.

Spinal segments were tested in vitro to measure range of motion (ROM). Thoracic segments were also tested with bipolar instrumentation to measure ROM and rod strain using a strain gage.

A subject-specific FEM of the spine, pelvis and ribcage of an in vivo asymptomatic subject was built. Spinal segments were extracted from it to reproduce the in-vitro mechanical tests. Experimental and simulated ROM and rod strain were compared. Then, the full trunk FEM was used to compare bipolar and all-screws instrumentations.

The FEM fell within 1° of the experimental corridors, and both in silico and in vitro instrumentation rods showed 0.01% maximal axial strain. Bipolar and all-screws constructs had similar maximal Von Mises stresses.

This work represents a first step towards subject-specific simulation to evaluate spinal constructs for neuromuscular scoliosis in children.

Keywords: neuromuscular scoliosis; bipolar technique; minimally invasive fusionless surgery; numerical model

[a] *Arts et Métiers Institute of Technology, Institut de Biomécanique Humaine Georges Charpak, Université Sorbonne Paris Nord, Paris, France.*

[b] *Paris Descartes University, Assistance Publique Hôpitaux de Paris, Pediatrics Orthopedics Department, Necker Hospital, 149 Rue de Sevres, 75015 Paris, France*.

Accepted Manuscript. Published in Journal of the Mechanical Behavior of Biomedical Materials.
DOI : https://doi.org/10.1016/j.jmbbm.2021.104797

1. Introduction

Neuromuscular spinal deformity (NMSD) is due to abnormal muscle tone and muscle imbalance which often starts in the first years of life. Progression of the deformity can lead to loss of sitting ability and respiratory insufficiency (Mayer, 2015). Therefore, those cases that progress without response to non-operative treatment (physiotherapy or bracing) must undergo early spinal surgery to stop the progression. Such an early fusion, however, can lead to cessation of trunk growth and of lung development, and this complex surgery presents a relatively high rate of complications: the meta-analysis by Sharma et al. (2013) reports 13% prevalence of mechanical complications such as implant breakage, loosening or cut-out of implant.

Growth-preserving surgical techniques have been developed to treat NMSD (Sarwahi et al., 2015); while they present the advantage of not stopping trunk growth, they can result in complication rates of 40-70% (Akbarnia et al., 2005; Bess et al., 2010)) including more than 20% which are due to implant failure or rod breakage (Thakar et al., 2018). Screw pull-out and implant migration are often due to the general poor health status of neuromuscular patients (malnutrition, osteopenia, etc.), while rod breakage may also occur in dynamic and heavy patients due to the long spinal constructs that are necessary to stabilize the whole spine.

Recently, a minimally-invasive fusionless surgical approach was developed (Gaume et al., n.d.; Miladi et al., 2018) as both an early surgical treatment that preserves growth and a definitive treatment avoiding arthrodesis at skeletal maturity. This technique is proposed as an alternative to arthrodesis which provides a high rate of complications in neuromuscular scoliosis (Rumalla et al., 2016). This method uses two fixation points for the construct: a pelvic anchoring with iliosacral screws and a proximal thoracic anchoring with supralaminar and pedicle hook claws. This differs from classical arthrodesis which employ pedicle screws at most (or all) vertebral levels to anchor the implant (Modi et al., 2008). Rod lengthening during growth can be achieved using the previous distal incision, thus respecting the minimal invasive philosophy of the technique.

While this method resulted in a mechanical complication rate similar to the lower end of fusion surgeries (30 % at 5 years follow-up (Gaume et al., n.d.)), the biomechanical behaviour of such “bipolar” construct, and its differences relative to an all-screws approach, has not been studied yet. Particularly, as rod breakage may be a clinical issue in the growing spine, whether an all-screw approach can limit mechanical stress in the rods is an open question. While iliosacral screws are known to be mechanically reliable (Miladi et al., 1997; Shabtai et al., 2017), the effect of only anchoring the instrumentation proximally with thoracic hooks in bipolar instrumentation is not known.

Numerical modelling has been widely used to simulate spine biomechanics, but model evaluation using *in-vivo* data is often challenging (Lafon et al., 2010, 2009). Furthermore, when considering numerical simulation of spinal instrumentation, implant or screw stresses are very important to evaluate risk of breakage, but such values are difficult to measure *in vitro* or *in vivo* to validate the model. However, implant strain can be measured experimentally, and these values are directly related to the stress.

A finite element model (FEM) of the scoliotic trunk has been previously described in the literature and it has been applied to simulate surgical approaches in severe scoliosis (Lafon et al., 2009). The aim of this work was to combine *in vitro* and *in vivo* data to improve and validate

Accepted Manuscript. Published in Journal of the Mechanical Behavior of Biomedical Materials.
DOI : https://doi.org/10.1016/j.jmbbm.2021.104797

this existing FEM of the spine, in terms of range of motion and bipolar implant strain, and to use the model to conceptually compare the stresses to which bipolar and all-screws implants are submitted.

2. Methods

2.1 General approach

A subject-specific FEM of the trunk of an asymptomatic subject was built, including spine, pelvis and ribcage. Models of the thoracic and lumbar spinal segments were extracted from this full model. Previous biomechanical tests were used to validate these segmental models in terms of range of motion (ROM) in three directions (Gaume et al., 2020). Cadaver tests on the thoracic sections also included testing of a bipolar instrumentation, and the comparison of instrumentation strain with the numerical results validated the FE model with regards to instrumentation. Finally, the full FEM of the subject, including pelvis and ribcage, was used to predict and compare instrumentation stress in two conditions: bipolar and all-screws instrumentations. Figure 1 shows the process, which is detailed hereafter.

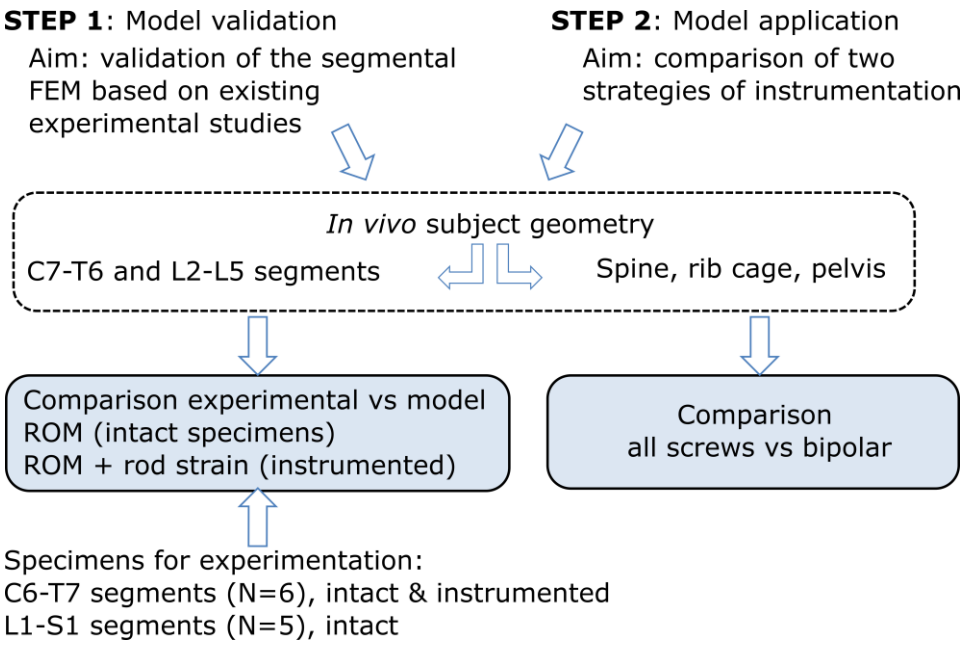

Figure 1. Schematic view of the methodological approach.

2.2 Model

The FEM of a thoracolumbar spine, ribcage and pelvis was generated based on previously described work (Descrimes et al., 1995; Lafage et al., 2004; Lafon et al., 2009; Vergari et al., 2015). Model's subject-specific geometry was obtained from standing biplanar radiography and

Accepted Manuscript. Published in Journal of the Mechanical Behavior of Biomedical Materials.
DOI : https://doi.org/10.1016/j.jmbbm.2021.104797

3D reconstruction (

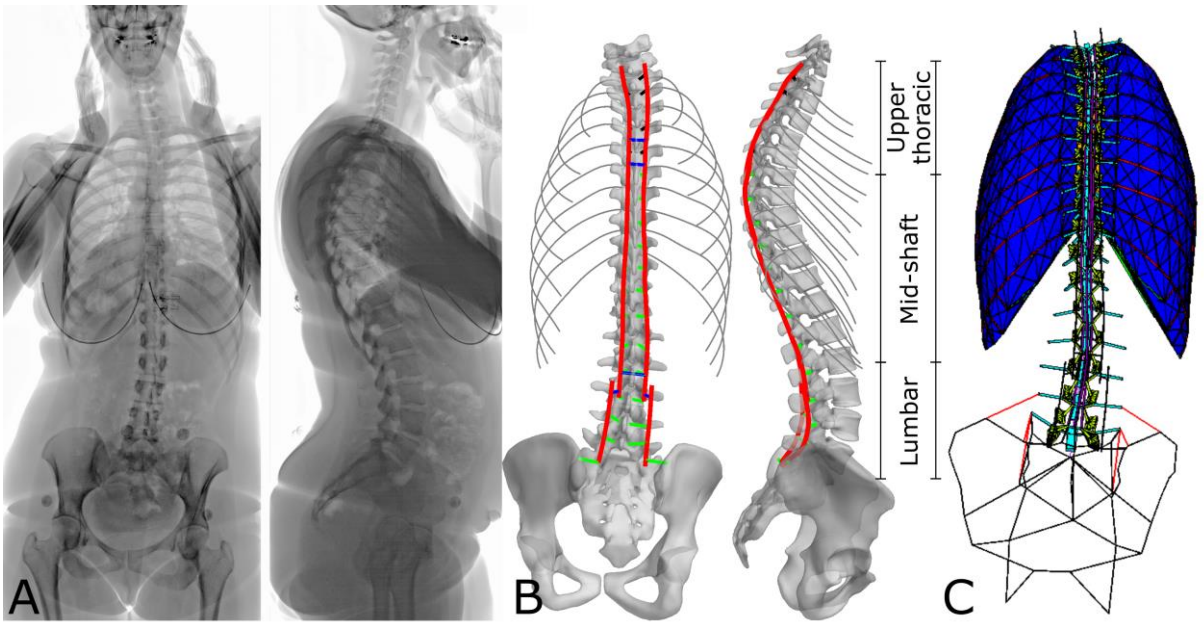

Figure 3A) of one asymptomatic female subject (40 years old) who underwent low dose biplanar X-Rays acquisitions, after ethical committee approval (CPP Ile de France VI 6036), and was retrospectively included in the study. The spine model consisted in the vertebral bodies, posterior arches, spinous processes, articular facets and intervertebral discs and ligaments. Bony structures were modelled by linear elastic behaviour (Poisson's ratio: 0.3, Elastic modulus: 1 GPa for the vertebral body, 3.5 GPa for spinous and transverse processes, and 5 GPa for other vertebral structures), while ligaments were multi-linear elastic (Chazal et al., 1985) and articular facets were non-friction contacts. Mechanical properties were previously detailed (Vergari et al., 2015), while the behaviour of intervertebral discs was approximated with a 3rd degree polynomial describing its moment (M) vs rotation (ΔΘ) relation in the form:

$$M = k_0.\Delta\theta.\left(1 + \left(\frac{\Delta\theta}{\theta_c}\right)^2\right) \qquad \text{(Equation 1)}$$

Here k_0 represents the initial segment stiffness and Θ_c is a stiffening parameter. These parameters were calculated by regression to fit the experimental moment vs rotation curves of thoracic and lumbar samples. When this mechanical property was implemented in the model, k_0 was utilized to calculate an equivalent elastic modulus (E) as follows:

$$E = k_0 \, {}^{L}/_{I} \qquad \text{(Equation 2)}$$

where I is the intervertebral second moment of area corresponding to the loading direction and L is the disc height. This allowed to adapt the mechanical behaviour relative to the subject-specific geometry.

Since only thoracic and lumbar segments were tested (see below), experimental data was not available for all discs; therefore, mechanical properties of the T6-L1 segment in the FEM was extrapolated from the available data

Accepted Manuscript. Published in Journal of the Mechanical Behavior of Biomedical Materials.
DOI : https://doi.org/10.1016/j.jmbbm.2021.104797

2.3 Segmental model evaluation

In order to evaluate crucial parts of the model, a thoracic (T1-T6, Figure 2C-D) and lumbar spinal segments (L2-L5) were extracted from this trunk model.

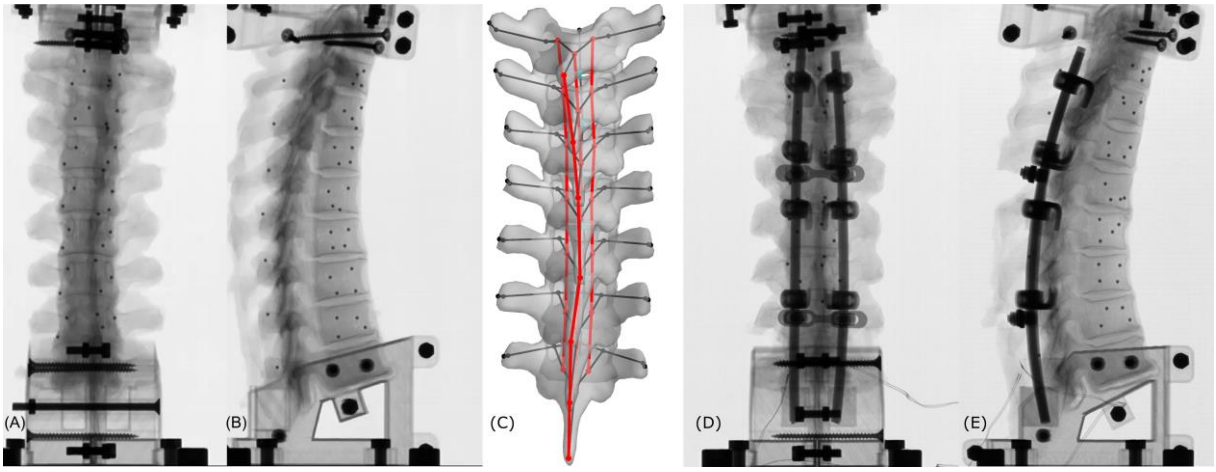

Figure 2. Frontal (A) and lateral (B) radiographies of a C7-T7 intact thoracic sample. Metal beads which were used to track vertebral motion are visible in the vertebral bodies and spinous processes. (C) Frontal view of the 3D reconstruction of T1-T7 vertebrae (volume models) and beam finite element model: bones are represented as black lines and ligaments in red. (D) and (E) show radiographs of an instrumented sample.

2.3.1 in vitro experiments

Existing in vitro experiments on five lumbar spinal segments (L1 to S1, 3 men, age range: 62-77 years) and six thoracic segments (C6 to T7, 6 men, age range: 43-63 years) were considered.

The mechanical testing protocol was previously described by Gaume et al. (2020), and is briefly described here. Upper (L1 or C6) and lower vertebrae (S1 or T7) were embedded in rigid blocks. The lower block was fixed while the upper block was attached to a custom testing rig equipped with a ± 10Nm load cell. Samples were loaded in flexion-extension (FE), lateral bending (LB) and torsion (TO) by applying pure moment: thoracic segments were loaded between ± 5 Nm in steps of 1 Nm while lumbar segments were loaded between ± 8 Nm in steps of 1.6 Nm.

Thoracic segments were then instrumented with a bipolar instrumentation and the segments were submitted to the same loading. Instrumentation spanned the whole segment from T1 to T7, and it was fixed with supralaminar and pedicle hooks fixed on two adjacent vertebrae (T1-T2 and T4-T5). Cross links were present at T3 and T6. The lower ends of the rods were embedded in the fixing block of the T7 vertebra. A strain gage was installed on the posterior face of the rod to measure its axial strain at the last loading step in FE. For motion measurement, the loading rig was installed within a biplanar radiographic device (EOS Imaging, Paris, France). Five steel beads of 2 mm diameter were inserted in each vertebra (Figure 2A-B. Biplanar radiographs were acquired at each loading step, and the beads were tracked in 3D to calculate intervertebral rotations in the three loading directions (Muth-seng et al., 2019). Furthermore, geometry of all vertebrae was reconstructed with previous validated methods

Accepted Manuscript. Published in Journal of the Mechanical Behavior of Biomedical Materials.
DOI : https://doi.org/10.1016/j.jmbbm.2021.104797

(Humbert et al., 2009). Second moment of area of each intervertebral disc was estimated by averaging the second moments of area of the adjacent vertebral endplates.

2.3.2 In vitro model evaluation.

The segmental spine models were used to reproduce the *in-vitro* tests boundary conditions. The vertebrae which were embedded in rigid blocks (C7, T6, L1, S1) were not considered, to avoid border effects. A virtual spinal instrumentation was also generated for the thoracic segment, including thoracic hooks (T1-T2 and T4-T5), to reproduce the instrumented *in-vitro* experimentation. Elastic modulus of instrumentation was 110 GPa (Niinomi, 1998). ROM of the intact thoracic and lumbar segments, as well as instrumented thoracic segment (Lafon et al., 2009), were compared to the experimental corridors. Longitudinal strain of the rod in FE of the thoracic segment was compared to the strain which was measured experimentally.

2.4 In-silico application

For the same *in vivo* subject above, the full trunk model was built, including spine, ribcage and pelvis (

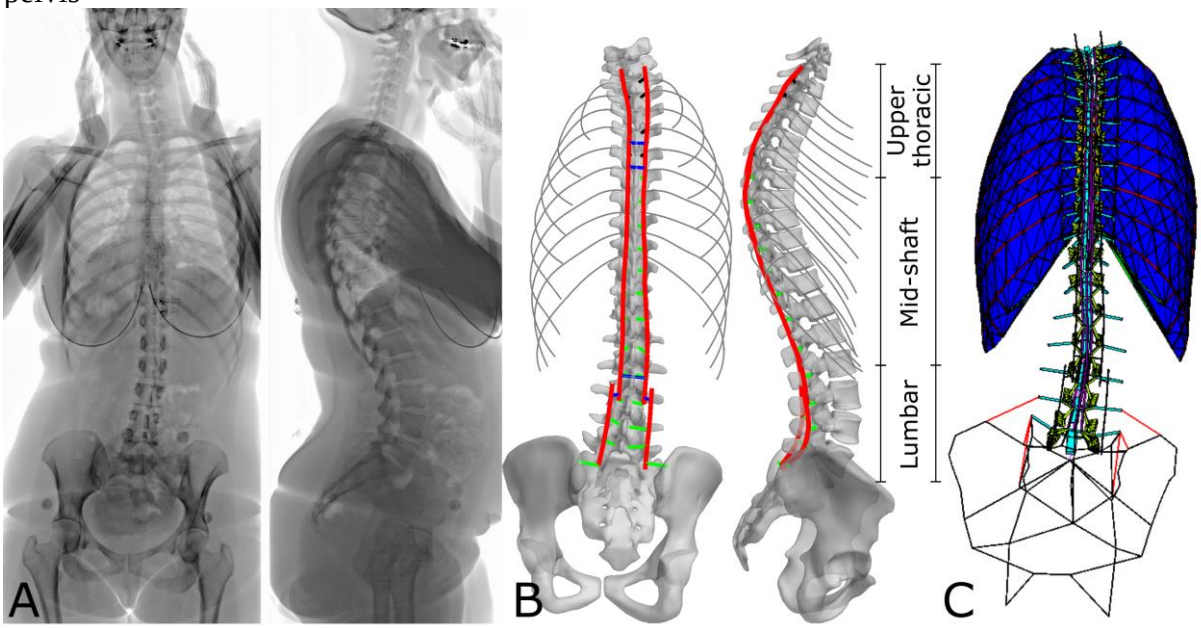

Figure 3). The virtual spinal instrumentation was extended from T1 to the pelvis, with the addition of ilio-sacral screws and a transverse element at L2 level. The instrumented trunk model was blocked at the pelvis, and rotations at the T1 vertebra were computed according to the hybrid method described by Panjabi et al. (2007), i.e., pure moments of ± 5 Nm were applied to the model, and the resulting rotations at the T1 vertebra were measured. These rotations (2.3° in flexion, 1.6° in right bending and 7.7° in torsion) were then imposed as boundary conditions in both instrumented configurations.

The model was then modified by adding pedicle screws at all vertebral levels between T6 and L5, and the simulations were repeated with the same boundary conditions. Maximal stress was

Accepted Manuscript. Published in Journal of the Mechanical Behavior of Biomedical Materials.
DOI : https://doi.org/10.1016/j.jmbbm.2021.104797

measured in the upper thoracic, mid-shaft and lumbar region of the two instrumentations (

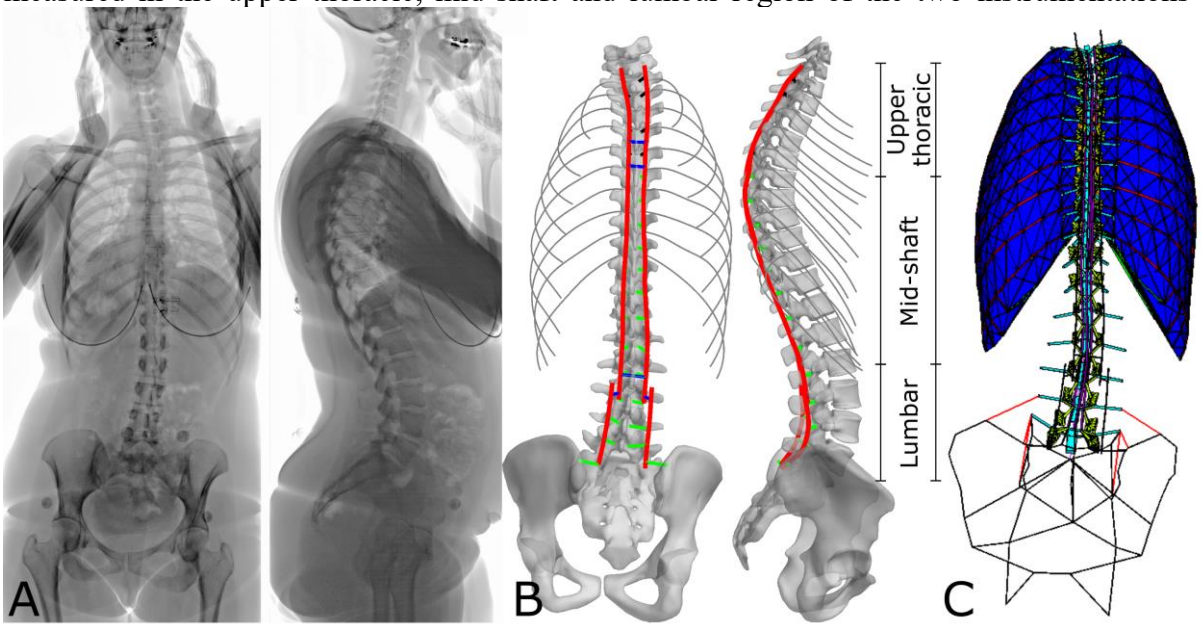

Figure 3).

The model was implemented in ANSYS V15 (Ansys Inc., Canonsburg, PA, USA).

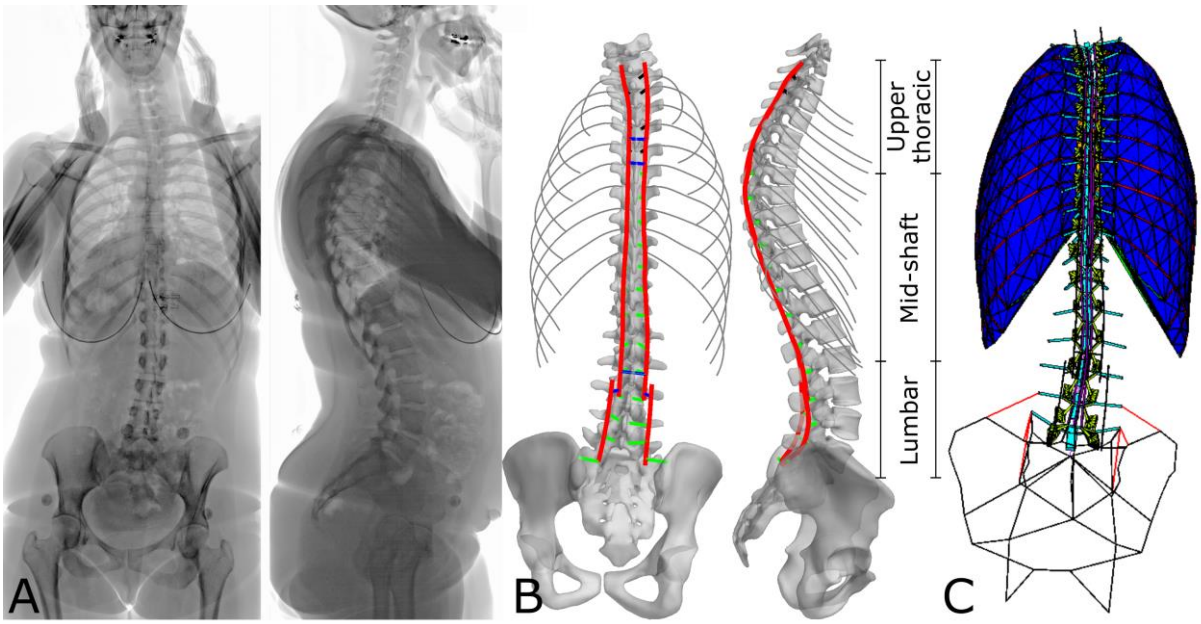

Figure 3. (A) Biplanar radiographies of a 40-years old healthy woman and (B) 3D reconstruction of her pelvis and spine, with the model of T1-S1 all-screws constructs. Rods are represented in red, crosslinks in blue, claw hooks in black and screws in green. Model of bipolar construct is similar, including iliosacral screws but without pedicle screws (in green). (C) Subject-specific finite element model.

Accepted Manuscript. Published in Journal of the Mechanical Behavior of Biomedical Materials.
DOI : https://doi.org/10.1016/j.jmbbm.2021.104797

3. Results

3.1 Intervertebral segment behaviour

Table 1 reports the values of k_0 and Θ_c approximating each intervertebral disc behaviour in the three loading directions. Loading curves were well approximated by the polynomial in Equation 1, with an $R^2 > 0.9$ in all loading conditions. Figure 4 shows the experimental corridor of thoracic (intact and instrumented) and intact lumbar spinal segments ROM, represented by the average ± 2*SD of all curves. Ranges varied between samples.

Table 1: Constants for polynomial approximation of disc properties (" indicates the same value as the cell above)

Segment	**Lateral bending**		**Flexion/Extension**		**Torsion**	
	k_0 (Nm/rad)	Θ_c (rad)	k_0 (Nm/rad)	Θ_c (rad)	k_0 (Nm/rad)	Θ_c (rad)
T1-L1	24.9	0.037	1.40 * 24.9	0.037	24.9	0.037
L1-L2	"	"	0.3 * 24.9	0.037	24.9	"
L2-L3	"	"	"	0.037	1.1 * 24.9	"
L3-L4	"	"	"	1.5 * 0.037	1.2 * 24.9	"
L4-L5	"	"	"	2.0 * 0.037	1.3 * 24.9	"
L5-S1	"	"	"	2.5 * 0.037	1.4 * 24.9	"

Accepted Manuscript. Published in Journal of the Mechanical Behavior of Biomedical Materials.
DOI : https://doi.org/10.1016/j.jmbbm.2021.104797

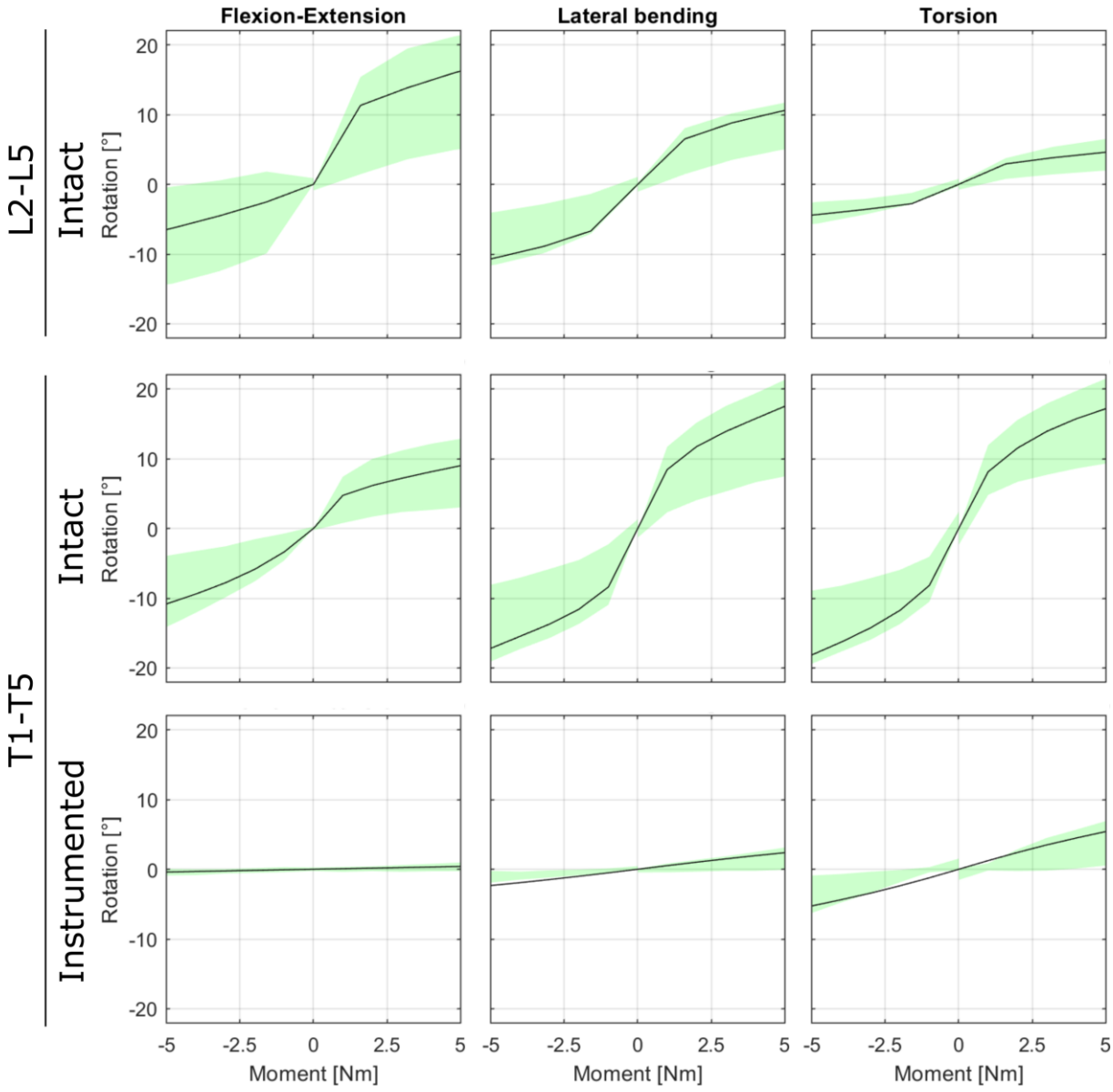

Figure 4. Range of motion of intact lumbar segments (L2-L5), and both intact and instrumented thoracic segments (T1-T5), comparing the experimental corridor (shaded areas, mean ± 2*SD) and the simulated tests using an *in-vivo* subject geometry (black line).

3.2 Model evaluation

Supplementary Content 1 shows an example of lateral inflexion *in vitro* and *in silico* test. Simulations based on *in-vivo* patient geometry (Figure 4, black curves) fell within the experimental range of 2SD for all intact configurations, and for all instrumented loadings except at maximal loading in LB and at initial negative loading in TO (Figure 4); in these cases,

Accepted Manuscript. Published in Journal of the Mechanical Behavior of Biomedical Materials.
DOI : https://doi.org/10.1016/j.jmbbm.2021.104797

simulated curves were outside of the two standard deviations experimental corridor by less than 1°.

Maximum axial strain obtained in the simulated rod at maximal FE loading was 0.010%, which is similar to the value measured by strain gauge in the thoracic rods (0.013 %).

3.3 Comparison of instrumentations

Supplementary Content 2-4 show comparison of the simulated behaviour of the two instrumentations under FE, LB and TO loadings, respectively. Maximal Von Mises stresses for the bipolar fixation were obtained in the upper thoracic region in LB (43.9 MPa), and in the lower lumbar region for the other two loadings (37.8 MPa in FE and 75.0 MPa in TO, Table 2). All-screws fixation yielded maximal stresses in the upper thoracic region for all loadings (34.8, 50.3 and 94.8 for FE, LB and TO respectively). Both instrumentations showed maximal stresses in torsion. Stress values was similar between the two fixations; the largest difference was obtained in torsion, where all-screws construct maximal stress was higher than the bipolar one by 20 MPa (26 %).

Figure 5 shows stress distributions; in both configurations, maximal stresses were concentrated near the fixations for all loadings. However, high stress was also present along the rods in torsion, while rod stress in FE and LB was lower.

Table 2. Comparison of maximum Von Mises stresses of the implant in the two configurations (bipolar and all-screws) and in different regions under three directions of imposed rotations. Plus signs at superscript indicate maximal values per loading and configuration.

	Bipolar			All-screws		
	Flexion	Lateral bending	Torsion	Flexion	Lateral bending	Torsion
Upper thoracic (MPa)	22.4	**43.9**$^{+}$	67.5	**34.8**$^{+}$	**40.3**$^{+}$	**94.8**$^{+}$
Mid-shaft (MPa)	32.8	31.0	69.1	17.1	29.1	86.3
Lower lumbar (MPa)	**37.8**$^{+}$	31.4	**75.0**$^{+}$	27.2	28.9	80.8

4. Discussion

Numerical models are the obvious means to compare different spinal instrumentations, but these models require prior validation against experimental data if their results are to be trusted. In this work, a subject-specific FEM of the intact and instrumented spine was evaluated against experimental data in terms of range of motion and rod axial strain, and then it was used to compare a bipolar and all-screws implants. In particular, it was not clear if only two anchoring points (distal and proximal), linked by long rods, could offer sufficient stability and resistance compared to more classical approaches which benefit from anchoring points at all vertebral levels. Indeed, growth-preserving surgery for NMSD could substantially benefit patients, but

Accepted Manuscript. Published in Journal of the Mechanical Behavior of Biomedical Materials.
DOI : https://doi.org/10.1016/j.jmbbm.2021.104797

they still present very high complication rates. The novel bipolar instrumentation with minimally-invasive surgery described by Miladi et al (2018) showed promising clinical results, but its mechanical behaviour has not been analysed yet.

Accepted Manuscript. Published in Journal of the Mechanical Behavior of Biomedical Materials.
DOI : https://doi.org/10.1016/j.jmbbm.2021.104797

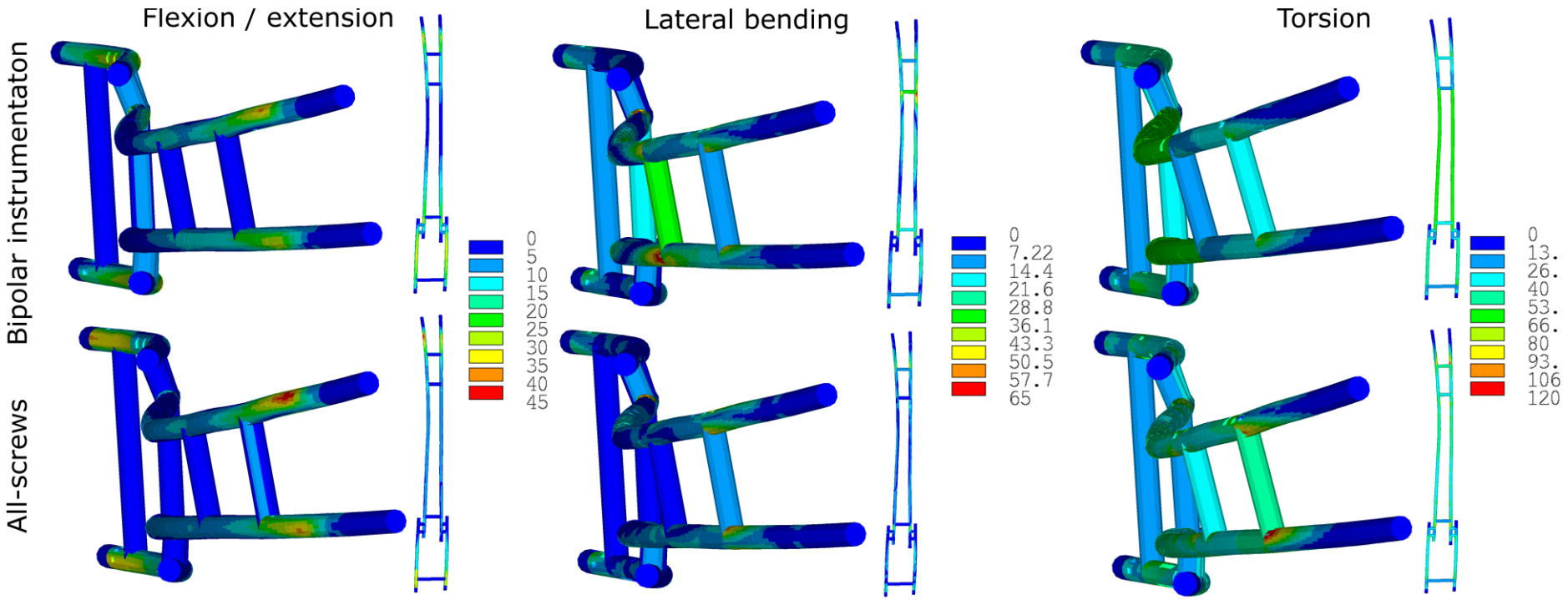

Figure 5. Von mises stress of the bipolar (first row) and all-screws instrumentations (second row) in flexion/extension, lateral bending and torsion, with a top view and lateral view in each loading. Stresses are concentrated near the anchoring points rather than along the rods. Color are different in each loading, showing that torsion presented the higher stresses.

Instrumentation was only tested *in vitro* on the thoracic spine, and the tested segment was relatively short (C7-T7) compared to the *in vivo* instrumentation, which would span the whole spine. This choices were made because the biomechanical behaviour and stability of thoracic hook fixation is much less studied than the distal fixation by iliosacral screws (Casaroli et al., 2020). The comparison of experimental and simulated axial rod strains is an important aspect of this works. Indeed, while stress is informative when comparing instrumentations, it is usually not feasible to validate the values obtained in a model. Strain, on the other hand, can be measured directly and it is directly related to stress, especially in linear elastic materials such as titanium.

The main limitation of this study is that different spinal specimens were used to characterize thoracic and lumbar discs, rather than full spines. Furthermore, the instrumented spine segment was shorter than the *in vivo* instrumentation. This is due to the difficulty of obtaining human cadaveric full spines without disc degeneration, osteophytes and other pathologies potentially affecting intervertebral mobility. Moreover, since the two tested segments did not represent the whole spinal column, mechanical properties of the T6-L1 segment in the FEM was extrapolated from the available data. Finally, gender of the subjects was not accounted for (Lang-Tapia et al., 2011). Nevertheless, the ROM of the upper thoracic region (T1-T7) was characterized in this work, a segment that is often neglected in the literature which mostly focused on the thoracic spine below T3 (Balabaud et al., 2002; Kuklo et al., 2008) or on shorter segments (Kingma et al., 2018; Wilke et al., 2017).

Another limitation is the use of cadaveric specimens of elderly subjects, when the instrumentation is mainly used in prepubertal or adolescent subjects. Not only the two differ in geometry and overall size, but also in mechanical properties, especially for the soft tissues. While this is a common limitation found in the literature, in this study the mechanical properties which were estimated from the mobility curves were normalized with the specimens' geometrical properties, and therefore they could be at least partially adapted to any subject's geometry. Moreover, in the present case of direct comparison between two instrumentation

Accepted Manuscript. Published in Journal of the Mechanical Behavior of Biomedical Materials.
DOI : https://doi.org/10.1016/j.jmbbm.2021.104797

configurations using the same trunk geometry (

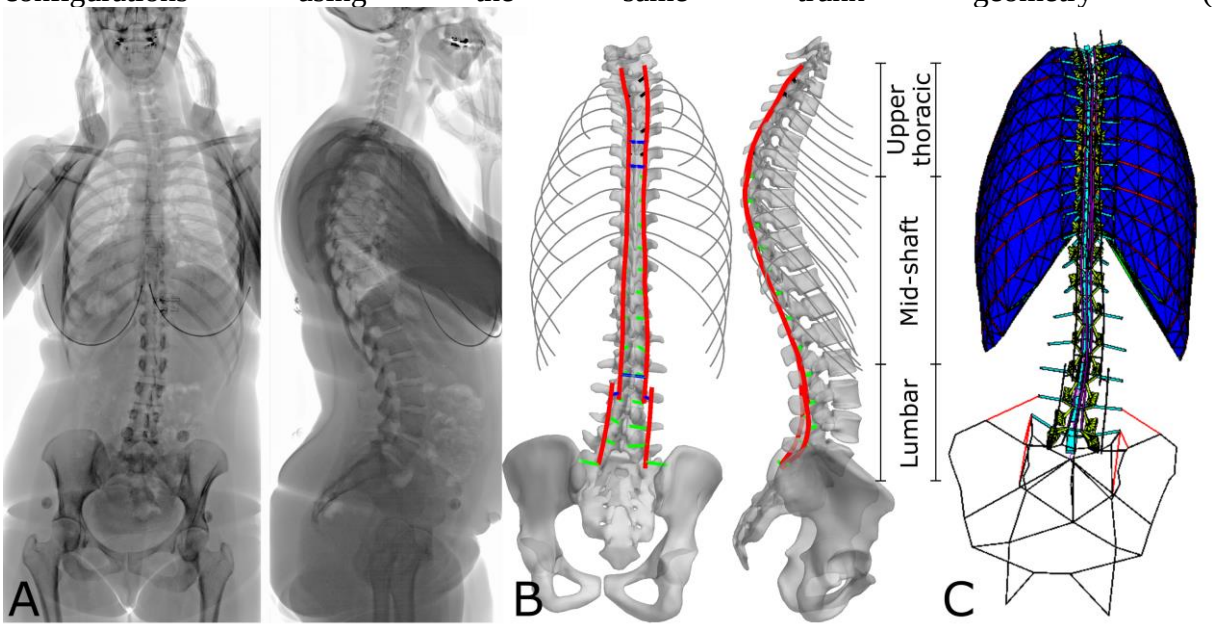

Figure 3), these limitations should have marginal effects on the results. Indeed, the claim of the present work is not the validation of the recent bipolar implant for use in adolescents, for which clinical validations already exist at 5-years follow-up, but to compare two instrumentation configurations. Besides, using an adult geometry in the simulation is closer to the experimental conditions, thus closer to the range of validation of the numerical model.

The results of the simulations reproducing the *in vitro* experiments are encouraging; the spinal geometry used to test the model was collected from *in vivo* data and was independent from the *in vitro* tests, and the results still fell within the experimental corridors of 2SD (Figure 4), which corroborates the model's reliability. In other words, the validation procedure is closer to a potential *in vivo* application than comparing simulation and experiments performed on the same specimens. Moreover, simulated rod strain corresponded to the measured one, providing a further degree of confidence in the model's results.

Finally, the trunk FEM was passive, as it did not include neuromuscular components, and it represented an adult's geometry. While implementing muscular action and control would lead to more realistic results, and instrumentation loadings, this is a common challenge in the existing literature, which still has to be overcome.

Simulations show that stresses were concentrated near the anchoring sites in both configurations (Figure 5). Comparisons with the literature are sparse because only few studies focused on the stress in long, growing rods *in situ*. For instance, Agarwal et al. found a maximal stress of 56 MPa applying 1 Nm moment in flexion (Agarwal et al., 2021), which is higher than the present results probably because those authors used a pre-stressed model with a follower load; in their case, the application of the flexion moment did not have any effect on implant stress. Ribesse et al. (2021) found maximal stresses near the distal anchoring site, at the thoracolumbar junction, while stresses were higher in the proximal anchoring site in the present work. However, shorter constructs were analysed in that work.

Results suggest that bipolar configuration shows similar stresses than all-screws configuration (Table 1, Figure 5). The bipolar technique overall demonstrated slightly higher stresses in FE

and LB, and lower stresses in TO than the all-screws configuration. Maximal Von Mises stress in flexion and lateral bending was 9% higher in bipolar than in all-screws, but the latter showed 26 % higher stress in torsion. It is not surprising that torsion loading yields higher stresses: the narrow rectangle formed by the thoracic and lumbar transverse elements and the two longitudinal rods does not offer high resistance to this loading. Nevertheless, both configurations were well below the yield strength of titanium medical grade alloys (about 850 MPa, Niinomi, 1998). Although the two constructs provide a similar order of magnitude of strains (Miladi et al., 2018), the *in vitro* and *in silico* approaches in the present work were limited to simple loading cases. Further *in-vivo* studies are necessary to go towards more realistic *in-vivo* loadings.

In conclusion, in this work a subject-specific FEM of the spine was evaluated in terms of ROM and implant strain against *in vitro* experiments: the model fell within the experimental curves in most conditions, and showed the same rod strain as the experimental measurement. Then, the model was completed with the subject's rib cage and pelvis and applied to compare bipolar and all-screws configuration. Results show that the two constructs were biomechanically similar, with similar locations and levels of maximal stress. Further work could aim at reproducing *in silico* the specific muscular activity patterns of NMSD patients. These patients present specific trunk deformities that can be reproduced with the subject-specific model described in this work, which represent a first step towards the simulation of proximo-distal spinal construct behaviour for NMSD patients.

5. Declaration of interest statement

The in vitro study was funded by EUROS company and the in vivo modelling by the BiomecAM chair program on subject-specific musculoskeletal modelling (with the financial support of ParisTech and Yves Cotrel Foundations, Société Générale, Proteor and Covea). The sponsors of this study were not involved in the design, collection, analysis of data or writing the report.

References

Agarwal, A., Kodigudla, M., Kelkar, A., Jayaswal, D., Goel, V., Palepu, V., 2021. Towards a validated patient-specific computational modeling framework to identify failure regions in traditional growing rods in patients with early onset scoliosis. North Am. Spine Soc. J. 5, 100043. https://doi.org/https://doi.org/10.1016/j.xnsj.2020.100043

Akbarnia, B.A., Marks, D.S., Boachie-Adjei, O., Thompson, A.G., Asher, M.A., 2005. Dual Growing Rod Technique for the Treatment of Progressive Early-Onset Scoliosis: A Multicenter Study. Spine (Phila. Pa. 1976). 30.

Balabaud, L., Gallard, E., Skalli, W., Lassau, J.-P., Lavaste, F., Steib, J.-P., 2002. Biomechanical Evaluation of a Bipedicular Spinal Fixation System: A Comparative Stiffness Test. Spine (Phila. Pa. 1976). 27.

Bess, S., Akbarnia, B.A., Thompson, G.H., Sponseller, P.D., Shah, S.A., El Sebaie, H., Boachie-Adjei, O., Karlin, L.I., Canale, S., Poe-Kochert, C., Skaggs, D.L., 2010. Complications of Growing-Rod Treatment for Early-Onset Scoliosis: Analysis of One Hundred and Forty Patients. JBJS 92.

Casaroli, G., Bassani, T., Brayda-Bruno, M., Luca, A., Galbusera, F., 2020. What do we know about the biomechanics of the sacroiliac joint and of sacropelvic fixation? A literature review. Med. Eng. Phys. 76, 1–12. https://doi.org/https://doi.org/10.1016/j.medengphy.2019.10.009

Chazal, J., Tanguy, A., Bourges, M., Gaurel, G., Escande, G., Guillot, M., Vanneuville, G., 1985. Biomechanical properties of spinal ligaments and a histological study of the supraspinal ligament in traction. J. Biomech. 18, 167–176.

Descrimes, J.L., Aubin, C.E., Skalli, W., Zeller, R., Danserau, J., Lavaste, F., 1995. Introduction des facettes articulaires dans une modélisation par éléments finis de la colonne vertébrale et du thorax scoliotique : aspects mécaniques. Rachis 7, 301–314.

Gaume, M., Persohn, S., Vergari, C., Glorion, C., Skalli, W., Miladi, L., 2020. Biomechanical cadaver study of proximal fixation in a minimally invasive bipolar construct. Spine Deform. 8, 33–80. https://doi.org/10.1007/s43390-019-00014-2

Gaume, M., Vergari, C., Khouri, N., Skalli, W., Glorion, C., Miladi, L., n.d. Minimally Invasive Surgery for Neuromuscular Scoliosis: Results and Complications at a Minimal Follow-up of 5 Years. Spine (Phila. Pa. 1976).

Humbert, L., De Guise, J.A., Aubert, B., Godbout, B., Skalli, W., 2009. 3D reconstruction of the spine from biplanar X-rays using parametric models based on transversal and longitudinal inferences. Med Eng Phys 31, 681–687. https://doi.org/10.1016/j.medengphy.2009.01.003

Kingma, I., Busscher, I., van der Veen, A.J., Verkerke, G.J., Veldhuizen, A.G., Homminga, J., van Dieën, J.H., 2018. Coupled motions in human and porcine thoracic and lumbar spines. J. Biomech. 70, 51–58. https://doi.org/https://doi.org/10.1016/j.jbiomech.2017.11.034

Kuklo, T.R., Dmitriev, A.E., Cardoso, M.J., Lehman, R.A.J., Erickson, M., Gill, N.W., 2008. Biomechanical Contribution of Transverse Connectors to Segmental Stability Following Long Segment Instrumentation With Thoracic Pedicle Screws. Spine (Phila. Pa. 1976). 33.

Lafage, V., Dubousset, J., Lavaste, F., Skalli, W., 2004. 3D finite element simulation of Cotrel-

Dubousset correction. Comput Aided Surg 9, 17–25. https://doi.org/VEKN2E8C7UGCJ8AW [pii]\n10.3109/10929080400006390

Lafon, Y., Lafage, V., Dubousset, J., Skalli, W., 2009. Intraoperative thraee-dimensional correction during rod rotation technique. Spine (Phila Pa 1976) 34, 512–519. https://doi.org/10.1097/BRS.0b013e31819413ec

Lafon, Y., Lafage, V., Steib, J.-P., Dubousset, J., Skalli, W., 2010. In vivo distribution of spinal intervertebral stiffness based on clinical flexibility tests. Spine (Phila Pa 1976) 35, 186–193. https://doi.org/10.1097/BRS.0b013e3181b664b1

Lang-Tapia, M., España-Romero, V., Anelo, J., Castillo, M.J., 2011. Differences on Spinal Curvature in Standing Position by Gender, Age and Weight Status Using a Noninvasive Method. J. Appl. Biomech. 27, 143–150. https://doi.org/10.1123/jab.27.2.143 10.1123/jab.27.2.143 10.1123/jab.27.2.143 10.1123/jab.27.2.143

Mayer, O.H., 2015. Scoliosis and the Impact in Neuromuscular Disease. Paediatr. Respir. Rev. 16, 35–42. https://doi.org/https://doi.org/10.1016/j.prrv.2014.10.013

Miladi, L., Gaume, M., Khouri, N., Johnson, M., Topouchian, V., Glorion, C., 2018. Minimally Invasive Surgery for Neuromuscular Scoliosis: Results and Complications in a Series of One Hundred Patients. Spine (Phila. Pa. 1976). 43, E968–E975.

Miladi, L.T., Ghanem, I.B., Draoui, M.M., Zeller, R.D., Dubousset, J.F., 1997. Iliosacral Screw Fixation for Pelvic Obliquity in Neuromuscular Scoliosis: A Long-Term Follow-Up Study. Spine (Phila. Pa. 1976). 22.

Modi, H.N., Suh, S.-W., Song, H.-R., Fernandez, H.M., Yang, J.-H., 2008. Treatment of neuromuscular scoliosis with posterior-only pedicle screw fixation. J. Orthop. Surg. Res. 3, 23. https://doi.org/10.1186/1749-799X-3-23

Muth-seng, C., Brauge, D., Soriau, N., Sandoz, B., Van den Abbeele, M., Skalli, W., Laporte, S., 2019. Experimental analysis of the lower cervical spine in flexion with a focus on facet tracking. J. Biomech. 93, 220–225. https://doi.org/https://doi.org/10.1016/j.jbiomech.2019.06.022

Niinomi, M., 1998. Mechanical properties of biomedical titanium alloys. Mater. Sci. Eng. A 243, 231–236. https://doi.org/https://doi.org/10.1016/S0921-5093(97)00806-X

Panjabi, M.M., 2007. Hybrid multidirectional test method to evaluate spinal adjacent-level effects. Clin. Biomech. 22, 257–265. https://doi.org/https://doi.org/10.1016/j.clinbiomech.2006.08.006

Ribesse, A., Ismail, K., Croonenborghs, M., Irda, N., Miladi, L., Jacques, P.J., Mousny, M., Pardoen, T., 2021. Fracture mechanisms in Ti and Co–Cr growing rods and impact on clinical practice. J. Mech. Behav. Biomed. Mater. 104620. https://doi.org/https://doi.org/10.1016/j.jmbbm.2021.104620

Rumalla, K., Yarbrough, C.K., Pugely, A.J., Koester, L., Dorward, I.G., 2016. Spinal fusion for pediatric neuromuscular scoliosis: national trends, complications, and in-hospital outcomes. J. Neurosurg. Spine SPI 25, 500–508. https://doi.org/10.3171/2016.2.SPINE151377

Sarwahi, V., Amaral, T., Wendolowski, S., Gecelter, R., Gambassi, M., Plakas, C., Liao, B., Kalantre, S., Katyal, C., 2015. Minimally Invasive Scoliosis Surgery: A Novel Technique in Patients with Neuromuscular Scoliosis. Biomed Res. Int. 2015.

https://doi.org/10.1155/2015/481945

Shabtai, L., Andras, L.M., Portman, M., Harris, L.R., Choi, P.D., Tolo, V.T., Skaggs, D.L., 2017. Sacral Alar Iliac (SAI) Screws Fail 75% Less Frequently Than Iliac Screws in Neuromuscular Scoliosis. J. Pediatr. Orthop. 37.

Sharma, S., Wu, C., Andersen, T., Wang, Y., Hansen, E.S., Bünger, C.E., 2013. Prevalence of complications in neuromuscular scoliosis surgery: a literature meta-analysis from the past 15 years. Eur. Spine J. 22, 1230–1249. https://doi.org/10.1007/s00586-012-2542-2

Thakar, C., Kieser, D.C., Mardare, M., Haleem, S., Fairbank, J., Nnadi, C., 2018. Systematic review of the complications associated with magnetically controlled growing rods for the treatment of early onset scoliosis. Eur. Spine J. 27, 2062–2071. https://doi.org/10.1007/s00586-018-5590-4

Vergari, C., Ribes, G., Aubert, B., Adam, C., Miladi, L., Ilharreborde, B., Abelin-Genevois, K., Rouch, P., Skalli, W., 2015. Evaluation of a patient-specific finite element model to simulate conservative treatment in adolescent idiopathic scoliosis. Spine Deform. 3, 4–11. https://doi.org/https://doi.org/10.1016/j.jspd.2014.06.014

Wilke, H.-J., Herkommer, A., Werner, K., Liebsch, C., 2017. In vitro analysis of the segmental flexibility of the thoracic spine. PLoS One 12, e0177823.

Accepted Manuscript. Published in Journal of the Mechanical Behavior of Biomedical Materials.
DOI : https://doi.org/10.1016/j.jmbbm.2021.104797

Supplementary Content legends

Supplementary Content 1: The animation shows an example of lateral inflexion in vitro and in silico test. Frontal and lateral radiographies are shown at each loading step. Metal beads which were used to track vertebral motion are visible in the vertebral bodies and spinous processes. Frontal and posterior views of T1-T7 vertebra 3D reconstruction (volume models) and beam finite element model are also shown: bones are represented as black lines, intervertebral discs in cyan and ligaments in red.

Supplementary Content 2: Flexion/extension loading of the spinal implant (T1-S1) in bipolar (A) and all-screws (B) configuration, in top, lateral and front views. Color scale represents Von Mises stresses (MPa). Spine, ribcage and pelvis were hidden for clarity.

Supplementary Content 3: Lateral inflexion loading of the spinal implant (T1-S1) in bipolar (A) and all-screws (B) configuration, in top, lateral and front views. Color scale represents Von Mises stresses (MPa). Spine, ribcage and pelvis were hidden for clarity.

Supplementary Content 4: Torsion loading of the spinal implant (T1-S1) in bipolar (A) and all-screws (B) configuration, in top, lateral and front views. Color scale represents Von Mises stresses (MPa). Spine, ribcage and pelvis were hidden for clarity.